REACTOR STRUCTURAL RESPONSE TO MOLTEN-FUEL-COOLANT INTERACTIONS

J.C. BRATIS, T.J. MARCINIAK

Engineering Mechanics Section, Reactor Analysis and Safety Division, Argonne National Laboratory, Argonne, Illinois 60439, U.S.A.

SUMMARY

In order to realistically determine the structural response of a Liquid Metal Fast Breeder Reactor to a Molten Fuel-Coolant Interaction (MFCI), an MFCI region was incorporated into the two-dimensional, hydrodynamic containment code, REXCO-H.

In this way, it is possible to account for the two-dimensional hydrodynamic response, as well as for the effect of vessels and plates, upon the expansion process in the MFCI region. Such an approach presents certain advantages: (1) rigid walls can be substituted by elastic-plastic vessels, (2) there is no need to adopt one-dimensional models, and (3) the fluid constraints need not be treated as either compressible or incompressible.

The MFCI model has been modified significantly in order to extend the usefulness of the code under a variety of conditions. The sodium equation of state has been improved using basic thermodynamic relations and recent data to incorporate temperature dependent properties. Heat transfer models available to describe the MFCI include not only a quasi-steady-state model, but also the parametric model.

The fuel heat of fusion is used in order to avoid the artificial increase in temperature employed to account for the full fuel energy. Non-homogeneous MFCI regions can be treated by assigning different parameters to each zone within a region, including volume fractions of fuel, sodium, steel and void, as well as initial fuel and coolant temperatures and fraction of molten fuel.

Several cases have been studied in order to delineate the effect of various parameters on the peak pressures generated in the MFCI zones. These include effect of initial fuel and coolant temperatures, void fraction, amount of molten fuel and/or vessel wall compliance. The response of a typical reactor configuration is evaluated for a given set of initial conditions, with three different ways of determining the energy release, including (a) the thermodynamic approach, (b) determination of a p-v using a one-dimensional model, and (c) the present model.

1. Introduction

Development of analytical methods to evaluate the consequences of postulated off-normal events in Liquid Metal Fast Breeder Reactors (LMFBR) has been a continuing effort over the past several years. The resulting codes and analyses cover the sequence of events from initiating conditions, such as local fuel failures, or whole core loss of flow through nuclear shutdown and subsequent evaluation of the consequences upon the primary containment. For example, codes are available used to study the initiating events [1] while others are used to continue the calculation through the nuclear shutdown of the reactor core [2]. Finally, the evaluation of the primary containment, which includes as major components the reactor vessel and head, is accomplished by utilizing a code such as REXCO [3,4]. Each of these are essentially dependent upon one another for input. For example, the VENUS code is used when the SAS code indicates significant fuel vapor pressures. Similarly, the REXCO codes come into play when VENUS or SAS2A calculations indicate the nuclear shutdown of the reactor due to some form of disassembly. At this point the state of the reactor is known in terms of energy content of fuel and sodium as well as the material composition of the core region. The potential mechanical work must be determined and appropriate input specified for the REXCO code, either in the form of P-V data or specific energy conversion models.

Local events resulting in MFCI's may be treated in a similar manner, except that it is not necessary to implement VENUS calculations. Also, these problems may be treated mechanistically such as is done in recent modifications to the SAS code [5]. However, in each of these calculations the effect, or interaction, between the MFCI zone and the surrounding structure either the subassembly duct or reactor containment is not usually taken into account. Similarly in whole reactor configurations using the REXCO code the actual process of heat transfer during the expansion of the core is not usually taken into account. Pressure-volume relationships developed separately are used to describe the work done during core expansion which neglect the response of the surroundings and their effect on pressures developed in the MFCI zone.

The purpose of this paper is to describe recent modifications to the REXCO-HT code [6] which is used to couple the heat transfer models which describe MFCI's or other similar phenomena to the hydrodynamic and structural response of reactor structures. Additions include improved heat transfer models such as the parametric model developed by Cho, et al. [7]. Along with the addition of the parametric model the heat of fusion of the fuel, non-condensible gas volumes, and vapor blanketing of the fuel particles have been taken into account. Each of these models are described in the following along with appropriate examples of applications to subassembly and reactor configurations. The main advantages of this approach consist of the ability to couple the heat transfer, hydrodynamic and structural response without having to make assumptions about the acoustic or inertial characterization of the fluid [7,8] and the elastic-plastic response of structures. This leads to a somewhat more realistic evaluation of the effects of MFCI's on the surroundings as well as the opposite effect. Another advantage of including heat transfer models into REXCO is that the characterization of the MFCI parameters may be changed from zone to zone so that temperature and material gradients present at the termination of the nuclear event may be considered. Also, all of the features of the REXCO code are available in the present version.

2. Model Development

2.1 Initial Considerations

The heat transfer model used to describe the molten fuel-coolant interaction in the initial version of the REXCO-HT code was the quasi-steady-state model developed by Cho, et al. [9]. Recent developments have led to the devising of more sophisticated models which include the fragmentation and mixing time of the fuel particles as well as time dependent heat transfer coefficients which allow somewhat higher initial heat transfer rates. The overall effect is to provide a model which may be used in parametric studies since the exact mechanisms of the fuel-coolant interaction process are not well known at this time, although much work is being performed to understand the process, especially under reactor operating conditions.

In REXCO-HT configurations the volumetric fractions of the fuel, coolant and non-condensible gases are specified for the MFCI zones. The remaining volume, if not specified, is assumed to be steel which does not take part in the heat transfer and expansion process directly but acts as an added mass. Along with this input the initial temperatures of the fuel and coolant are given as well as the fuel particle size. As a further option, an initial sodium vapor fraction may be included but care must be taken that the sodium temperature is correctly given. All heat transfer calculations made are based on one gram of sodium and the fuel and sodium within an MFCI zone are assumed to be at a uniform, but different, temperature, i.e., no fuel or sodium temperature gradients within a zone are allowed. However, adjacent MFCI zones may have both fuel and sodium at different temperatures but no heat transfer is allowed across a zonal boundary.

Calculation of the zonal pressure based on the heat transfer and volumetric changes per time step is dependent upon adequate treatment of the sodium equation of state. The present version of the REXCO-HT code is thermodynamically consistent and includes temperature dependent sodium properties.

2.2 Heat Transfer Models

The quasi-steady-state model (QSS) used in REXCO-HT assumes that the only resistance to the heat transfer is due to the thermal conductivity of the fuel. The heat transfer rate is given by the relation

$$\dot{q} = A_o h(T_f - T) = \frac{3w}{\rho_f r} h(T_f - T) \tag{1}$$

where

$$k = k_f / r \tag{2}$$

A more sophisticated version, the ANL parametric model, introduces the fragmentation and mixing time constant, t_m, as a parameter as well as a time dependent heat transfer coefficient. The heat transfer rate is given by

$$\dot{q} = \frac{3w}{\rho_f r} h' \left[1 - \exp(-t/t_m)\right](T_f - T) \tag{3}$$

where

$$h' = \frac{k_f}{\sqrt{\pi \alpha_f t}} + \frac{k_f}{r} \tag{4}$$

Sodium vapor produced during the fuel-coolant interaction is likely to surround the fuel particles and thus effectively reduce the heat transfer from the fuel to the sodium. This is an important mechanism that reduces the rate at which heat is transferred to the sodium and consequently the work produced by the FCI zone expansion. In order to account for this reduction, two options have been incorporated into the REXCO-HT code. They can be used with

either the quasi-steady-state model or the ANL parametric model. In the first option (a), the thickness of the vapor blanket is calculated for each time step and the resistance to heat transfer by conduction through the vapor blanket is included in the estimate of the heat transferred in a time step. In the second option (b), a fraction of the fuel particles equal to the volumetric fraction of sodium vapor (compared to the total volume of sodium) is assumed not to participate in the heat transfer process. Option (a) is expected to underestimate the heat transfer because it ignores the convective heat transfer through the vapor blanket. One could introduce an effective thermal conductivity for the sodium vapor that would account, as a first approximation, for the convective effects.

After the heat transfer rate has been calculated for the (n+1)th step, the heat transferred from the fuel to the sodium is given by

$$\Delta Q = \dot{q}\Delta t \tag{5}$$

and the change of the fuel temperature is found from the relation

$$\Delta Q = c_f w \Delta T_f \tag{6}$$

In the event that the fuel is at its melting temperature, the heat of fusion is taken into account by introducing the fraction of the solidified fuel and not allowing a change in fuel temperature until all fuel is solidified. This feature allows a less conservative approach than that of increasing the initial fuel temperature to account for the heat of fusion.

2.3 Sodium Equation of State

For the (n+1) time step, the change of volume of a zone, ΔV, is calculated in the hydrodynamic subroutine of REXCO and the heat transferred to the sodium has been estimated using the desired heat transfer model. Since fuel and steel volumes are assumed incompressible, the volume change of a zone is due to the sodium and the fission gas present in the zone. The fission gas is assumed to be at the same temperature as the sodium. In order to find the pressure at time t_{n+1}, two cases will be considered: (1) the sodium at time t_n is in the liquid phase region, and (2) at time, t_n, the sodium is in the two-phase region.

2.2.1 Sodium in the Liquid Phase Region

When the sodium is in the liquid phase region, the following thermodynamic relations are employed, written in finite difference form:

$$c_p \Delta T - T\, V_{Na}\, \alpha_p \Delta P = \Delta Q \tag{7}$$

$$(\alpha_p V_{Na} + w_g \frac{R}{P})\, \Delta T - (\beta_T V_{Na} + w_g \frac{RT}{P^2})\, \Delta P = \Delta V\ . \tag{8}$$

From these, the changes in temperature, ΔT, and pressure, ΔP, are calculated and the pressure and temperature at time t_{n+1} are found using

$$P_{n+1} = P_n + \Delta P\ , \tag{9}$$

and

$$T_{n+1} = T_n + \Delta T\ . \tag{10}$$

This sequence will continue until such time as the sodium reaches its saturation pressure, corresponding to the local sodium temperature.

2.2.2 Sodium in the Two-Phase Region

When the sodium pressure corresponds to the local saturation pressure, P_σ, the following thermodynamic relations are used

$$\left\{\left(\frac{dh_\ell}{dT}\right)_\sigma (1-x_n) + \left(\frac{dh_v}{dT}\right)_\sigma x_n - V_n \frac{dP_\sigma}{dT}\right\} \Delta T + \Delta h_{\ell v}\Delta x = \Delta Q \tag{11}$$

$$\left\{\left(\frac{dV_\ell}{dT}\right)_\sigma (1-x_n) + \left(\frac{dV_v}{dT}\right)_\sigma x_n - w_g \frac{RT}{P^2} \frac{dP_\sigma}{dT} + w_g \frac{R}{P}\right\} \Delta T + \Delta V_{\ell v}\Delta x = \Delta V \tag{12}$$

Using eqs. (11) and (12), in which the heat transferred and the change in volume are known, the sodium temperature at time t_{n+1}, is found using eq. (10), while the sodium vapor quality is found by

$$x_{n+1} = x_n + \Delta x \ , \tag{13}$$

where Δx is the incremental change in the vapor quality.
The pressure is then calculated from

$$P_{n+1} = P_\sigma(T_{n+1}) \ , \tag{14}$$

since the pressure is the saturated vapor pressure of the sodium in the zone and corresponds to the local sodium temperature.

3. Sample Cases

The following describes the results of three different configurations which were investigated to demonstrate the MFCI models used in the REXCO-HT code. The first configuration is examined in order to gain some insight into the effect of various parameters while the other two configurations refer to a subassembly and to a full reactor in order to demonstrate the possible effects of MFCI's on reactor structures.

3.1 Simple Model

A simple model consisting of four zones is investigated for different initial conditions which are listed in Table I. As shown in the insert of Fig. 1, the FCI region is represented by one zone, while the other three consist of sodium at the same temperature as the initial sodium temperature in the FCI zone. The cylinder wall is assumed rigid except for case 9 in which a flexible steel wall is assumed with a thickness of 0.254 cm. For the heat transfer calculation, the quasi-steady-state model is utilized.

Cases 1, 2, and 3 were run in order to study the effect of the initial sodium temperature. Figure 1 presents the pressure histories for these cases. It is seen that the peak pressure increases with decreasing initial sodium temperature. This is so because: (i) the isothermal compressibility of sodium decreases with decreasing temperature ('harder' sodium), and (ii) the heat-transfer rate from the fuel to the sodium increases with decreasing sodium temperature, due to the higher temperature difference. The onset of vaporization and condensation is similar in the three cases, the only difference being the lower pressure at which it occurs for lower initial sodium temperatures. The onset of vaporization coincides with the unloading time. For lower sodium temperatures, the speed of sound is increased, and the unloading time decreased. Hence, the onset of vaporization takes place (at earlier times) for lower sodium temperatures. The second pressure peak is higher for lower sodium temperatures ('harder' sodium). In Fig. 2, the sodium temperature in the FCI zone is presented as a function of time for cases 1, 2, and 3. The higher initial temperature difference between fuel and sodium in case 3 causes a higher heat transfer rate, and therefore a faster increase in the sodium temperature than in cases 1 and 2.

Effects of sodium vapor blanketing are examined in cases 4, 5, and 6. The initial

conditions for these cases are the same as in case 1. Vapor blanketing option (a) is employed in case 4, while case 5 uses option (b). In case 6, option (a) is utilized with an effective vapor thermal conductivity ten times higher than the actual thermal conductivity. Figure 3 presents the pressure in the FCI zone as a function of time. It is seen that for all three cases, the pressure history for the initial period, before vaporization starts, is the same as in case 1. Since there is no vapor present, there are no blanketing effects. The effect of vapor blanketing becomes significant at a later time. As was already discussed, model (a) underestimates the heat transfer and this is seen in the lower pressures exhibited in Fig. 3. Introduction of an effective sodium vapor thermal conductivity ten times greater than the actual, gives results which are in close agreement with model (b). The sodium temperature in the FCI zone is given in Fig. 4 for cases 1, 4, 5, and 6. Sodium pressure and temperature are directly related at later times, since the pressure in the FCI zone is the sodium saturation pressure for the corresponding temperature.

For the purpose of studying the effect of artificially increasing the fuel temperature in order to account for the heat of fusion as compared to accounting for it in the program, case 7 was run. The initial fuel temperature was increased by 635 K, while the other initial conditions were taken as in case 1. The effect on the pressure is shown in Fig. 5, where the peak value is just below 390 bar in comparison to 290 bar obtained for case 1. This result shows, as expected, that the increase of the fuel temperature, in order to account for the heat of fusion, overestimates the pressure values. The effect on the sodium temperature is also shown in Fig. 5. Due to the higher fuel temperature, the heat transfer rate - and therefore the rate of sodium temperature increase - is higher as compared to case 1.

In case 8, a small amount of fission gas was assumed initially in the FCI zone (10% at 1 bar). The rest of the initial conditions were taken to be the same as in case 1. As seen in Fig. 6, the pressure rises slowly, since the expanding liquid sodium simply compresses the compliant fission gas, and peaks at approximately 87 bar.

The effect of a flexible wall is demonstrated with case 9. The initial conditions are the same as in case 1. In Fig. 7, the pressure history of the FCI zone is presented for case 9 and for case 1, in which a rigid wall was assumed. The presence of the flexible wall reduces the peak pressure from 293 bar to 215 bar. It is worth noting that the presence of a flexible wall creates a second pressure pulse with a high peak pressure.

3.2 Subassembly Response to MFCIs

An interesting application of the REXCO-HT code is to investigate the influence of various initial and boundary conditions on the possible response of subassemblies to local fuel-coolant interactions. The configuration used in this example is shown in Fig. 8 which nominally represents a typical LMFBR subassembly in that the cross-sectional area and wall thickness are maintained. However, since this model is cylindrical, the strength of a hexagonal-shaped subassembly wall is overestimated, but for the present purposes, this is adequate to illustrate general trends. Several cases were run mainly to demonstrate the effect of the heat transfer model on the pressure-time history, as well as the response of the subassembly wall and surrounding environment. The heat transfer models used are the quasi-steady-state model (QSS) and the parametric model (PAR), with a zero mixing and fragmentation time. In general, the QSS model corresponds to the parametric model with a fragmentation and mixing time constant of about 3 ms. The properties of the cylindrical wall

correspond to those of 316 stainless steel at 811 K, and a fluence of about $2 \times 10^{23} \phi t$. The yield strength is 3.93×10^3 bar, and Young's modulus is 1.6×10^6 bar, while the ultimate stress is 5.86×10^3 bar at a strain of 1.06 percent.

Initial and boundary conditions are given in Table II. The first three cases use the quasi-steady-state model, while the last three use the parametric model. Cases S1 and S4 are rigid wall models, while the other cases have a flexible wall with either argon gas or liquid sodium in the gap between wall and rigid boundary. These last cases are illustrative of the effect of the surroundings on the response of the subassembly wall.

Figure 9 is the pressure-time history in the center of the MFCI region using the QSS heat transfer model. Little effect is noted since the maximum pressure does not exceed the yield strength of the wall. Slight effects are seen at short times, but the total impulse of these pressure pulses is small. It is interesting to note that in case S2, the peak vapor pressure is slightly higher than in the rigid wall case. This is due to a rebounding effect due to the relatively incompressible sodium outside the wall compared to argon gas. Sodium temperature and vapor fraction histories are the same for these cases. Small differences that appear at later times can be attributed to the different energies absorbed by the subassembly wall.

High heat transfer rate effects on the pressure-time history of the MFCI zone are demonstrated in Fig. 10 in which the parametric model with zero mixing and fragmentation time is used. The initial peak pressure, which is the same in all three cases, is 2.4 kbar. A second pressure peak is noted in all three cases and corresponds to the reflected wave from the rigid boundary. The second pressure pulse is reduced in magnitude and delayed in time as the radial surroundings are made more compliant. There is little qualitative difference between cases S4 and S5, showing that a flexible wall surrounded by a relatively incompressible fluid such as sodium behaves quite rigidly, even in the presence of a fairly large transient pressure. However, compliant materials, such as argon gas, allow radial movement of the wall, which in this case, fails at about 0.4 ms. This can be an important effect, if one is to evaluate the ability of a subassembly can to resist failure due to a local molten fuel-coolant interaction. Figures 11 and 12 show the coolant temperature and vapor fraction in cases S4 through S6. The temperature drops rapidly in case S6, due to the rapid radial expansion of the MFCI zone.

3.3 Full Reactor Configuration

The full reactor configuration employed in this example is shown in Fig. 13. Four different cases were investigated with their initial conditions given in Table III. For the first case (R1), a modified Hicks - Menzies model [10] was used in obtaining a P-V curve for the core. In this model, fuel and sodium are assumed to reach thermal equilibrium before the core expansion starts. During the core expansion, the fuel is thermally decoupled from the sodium so that essentially no heat is transferred during the expansion. This calculation is expected to be conservative because of the assumption of thermal equilibrium between fuel and sodium before the core expansion starts, but not as conservative as the basic Hicks-Menzies model [11].

In the second case (R2) the FCI model was utilized as described in Section 2. Because of the assumption that the FCI zones do not exchange heat with the surroundings and that the heat-transfer coefficient remains unchanged even when sodium vapor is present, it is expected that this case will yield more energy than the modified Hicks - Menzies model. Allowing

heat transfer from the fuel to the sodium during the core expansion process will have as a result a higher amount of heat transfer than in Case R1.

Case R3 is expected to give more realistic results than the previous cases because the sodium vapor blanketing is being taken into account (option b). Case R4 is similar to Case R2 except for the presence of 10 percent cushion gas. One other case was investigated in which the P-V relation was obtained from the one dimensional model of Cho et al. [9]. Unfortunately, due to the two dimensional model employed here, the core expands faster than in the one dimensional model resulting in a rapid decrease of the core pressure. The inertial behavior of the two models is quite different due to the radial motion allowed in the present model.

In Fig. 14 the pressure histories of the core are presented. The pressure curve for Case R1 is not smooth because the P-V curve obtained from the modified Hicks - Menzies model was fed into the code by a number of (P,V) points. It is seen that the pressure pulse for Cases R2 and R3 is identical; since sodium vapor is not present, there is no difference between the two cases. The second pressure pulses differ slightly. For Case R2, it appears a little earlier and also has a somewhat higher pressure peak. This is so because there is sodium vapor present in the core during the time interval between the two pressure pulses and this reduces the amount of heat being transferred. The presence of cushion gas changes entirely the pressure history in the core. There is only one pressure pulse in case R4 which appears at a much later time and with a pressure peak which is 60 percent lower than in Cases R2 and R3.

In Fig. 15 the deformations of the Lagrangian grid are shown at time $t = 17.5$ ms. It is seen that the core has expanded more for Case R1 and this agrees well with the shape of the P-t curve shown in Fig. 14. For Case R3, the core expansion is the smallest because of the sodium vapor blanketing effect on the heat transfer. Finally, the core expansion energy and the heat transferred are presented in Fig. 16 as a function of time. The modified Hicks - Menzies model releases more energy at the beginning, tapering off at later times. In contrast, the R2 model releases less energy at the beginning but the rate of energy release increases with time. It is expected that at later times the core expansion work for Case R2 will become larger than the work for Case R1 for the reasons explained above. The lower core expansion work exhibited in Case R3 reflects the heat-transfer reduction due to sodium vapor blanketing.

4. Conclusions

1. Direct treatment of reactor heat transfer phenomena such as molten fuel-coolant interactions in a hydrodynamic containment code such as REXCO is desirable since this approach provides a direct coupling of all effects without having to resort to decoupled energy conversion calculations. Inclusion of models which describe molten fuel coolant interactions allows the consideration of the MFCI pressure pulses on reactor structures such as fuel subassemblies and the reactor primary containment. Effects due to coolant vapor formation can be rudimentarily taken into account with vapor blanketing models and the inclusion of the fuel heat of fusion negates the need to artificially increase the fuel temperature to account for the energy content of the fuel.

2. Calculations demonstrating the effect of various parameters on the MFCI process show that vapor blanketing can have a strong effect in reducing the heat transfer rate and that if radial motion is taken into account vaporization can occur earlier and this reduces the

heat transferred from the fuel to the sodium.

3. In subassembly configurations relatively slow heat transfer rates produce relatively low initial pressures and result in little hoop strain in the walls with little effect contributed by the surrounding medium. However, for very large heat transfer rates resulting in relatively high pressures the surroundings become important in assuring the survivability of the walls. This indicates that finite element codes, being developed to treat the dynamic response of subassembly ducts to internal pulses originating from local MFCI's should take into account the sodium coolant in the gap between subassemblies as well as the next row of subassemblies.

4. A more realistic response of reactor containments to whole core events may be accomplished through the use of coupled MFCI models. The resulting energy partitioning could be changed significantly and may well provide an extra margin of safety in the evaluation of the system.

Nomenclature

A_o	fuel area per gram of sodium
C_f	specific heat of fuel
C_p	specific heat of sodium under constant pressure
h, h'	heat transfer coefficient from fuel to sodium
h_ℓ, h_v	enthalpy of liquid and vapor sodium
k	Thermal conductivity
P	pressure
$\dot{q}$	heat transfer rate per gram of sodium
r	fuel particle radius
R	fission gas constant
t	time
T	sodium temperature
V	specific volume
w	fuel to sodium mass ratio
w_g	fission gas to sodium mass ratio
x	vapor quality of sodium

Greek Symbols

α_f	fuel thermal diffusivity
α_p	sodium thermal expansion coefficient
β_T	sodium isothermal compressibility
ρ	density

Subscripts

f	fuel value
ℓ	liquid sodium value
ℓv	difference between liquid and vapor values
v	sodium vapor value
σ	saturation value

References

[1] Dunn, F. E., Heames, T. J., Pizzica, P. A. and Fischer, G., "The SAS2A LMFBR Accident Analysis Code," Proc. of Conf. on New Developments in Reactor Math. and Applications, pp. 120-127, March 29-31, 1971.

[2] Jackson, J. F. and Nicholson, R. B., "VENUS-II: An LMFBR Disassembly Program," USAEC Report ANL-7951, (September 1972).

[3] Chang, Y-W., Gvildys, J. and Fistedis, S. H., "Two-Dimensional Hydrodynamic Analysis for Primary Containment," USAEC Report ANL-7498 (November 1969).

[4] Chang, Y-W. and Gvildys, J., "Dynamic Response of Reactor Containment to High Energy Excursion," Proc. of First Int. Conf. on Structural Mechanics in Reactor Technology, 3E, pp. 169-187, EUR 4820 d-f-e, 1972.

[5] Smith, L. L., Travis, J. R., Stevenson, M. G., Dunn, F. E. and Fischer, G. J., "SAS/FCI, A Fuel-Coolant Interaction Model for LMFBR Whole-Core Accident Analysis," Proc. of Conf. on Math. Models and Computational Techniques for Analysis of Nuclear Systems, April 9-11, 1973. (To be published).

[6] Marciniak, T. J., "Heat Transfer in Post Burst Accident Models," Proc. of First Int. Conf. on Struct. Mech. in Reactor Technology, 3E, pp. 189-206, EUR 4820 d-f-e (1972).

[7] Cho, D. H., Chen, W. L., and Wright, R. W., "Pressure Pulses and Mechanical Work from Molten Fuel-Coolant Interactions: A Parametric Study, "Trans. Am. Nuc. Soc., 14, 1, 290 (1971).

[8] Coldarola, L., "A Theoretical Model for the Molten Fuel-Sodium Interaction in a Nuclear Fast Reactor," Nuclear Engineering and Design, 22, pp. 175-211 (1972).

[9] Cho, D. H., Ivins, R. O., and Wright, R. W., "Pressure Generation by Molten Fuel-Coolant Interactions under LMFBR Accident Conditions," Proc. of Conf. on New Developments in Reactor Mathematics and Computations, Idaho Falls, Idaho, March 29-31, 1971. USAEC Rep. CONF-710302, pp. 25-49.

[10] Hesson, J. H., Sevy, R. H. and Marciniak, T. J., "Post Accident Heat Removal in LMFBR's: In-Vessel Considerations," USAEC Report ANL-7859 (September, 1971).

[11] Hicks, E. P. and Menzies, D. C., "Theoretical Studies on the Fast Reactor Maximum Accidnet," Proc. of the Conf. on Safety, Fuels and Core Design in Large, Fast Power Reactors, Oct. 11-14, 1965. USAEC Report ANL-7120.

TABLE I. Initial Condition of the FCI Zone

Case	Fuel Temp. T_f, °K	Coolant Temp. T_{Na}, °K	Volumetric Fraction of Fuel, α_f	Volumetric Fraction of Coolant, α_{Na}	Volumetric Fraction of Cushion Gas, α_g	Fraction of Solidified Fuel --	Remarks
1	3115	1200	0.5	0.5	0	0	
2	3115	1000	0.5	0.5	0	0	
3	3115	800	0.5	0.5	0	0	
4	3115	1200	0.5	0.5	0	0	Blanketing; Option (a)
5	3115	1200	0.5	0.5	0	0	Blanketing; Option (b)
6	3115	1200	0.5	0.5	0	0	Blanketing; Option (a) with $k_{eff} = 10.k_v$.
7	3750′	1200	0.5	0.5	0	0	Artificially higher fuel temperature.
8	3115	800	0.45	0.45	0.1	0	
9	3115	1200	0.5	0.5	0	0	Flexible wall.

TABLE II. Initial and Boundary Conditions

Case	Fuel Temp. °K	Coolant Temp. °K	Fuel Volumetric Fraction αf	Sodium Volumetric Fraction αNa	Fraction of Solidified Fuel Fuel	Wall Material	Gap Material	Heat Transfer Model
1	3115	672	.5	.5	0	RIGID	-	QSS
2	3115	672	.5	.5	0	316SS	Na	QSS
3	3115	672	.5	.5	0	316SS	Ar	QSS
4	3115	672	.5	.5	0	RIGID	-	Par.(t_m = 0.)
5	3115	672	.5	.5	0	316SS	Na	Par.(t_m = 0.)
6	3115	672	.5	.5	0	316SS	Ar	Par.(t_m = 0.)

TABLE III: Initial Conditions for the Full Reactor Configuration

Case	Fuel Temp. T_f, K	Coolant Temp. T_{Na}, K	Volumetric Fraction of Fuel α_f	Volumetric Fraction of Coolant α_{Na}	Volumetric Fraction of Cushion Gas a_g	Remarks
R1	3400	900	0.208	0.393	0	Hicks and Menzies P-V
R2	3400	900	0.208	0.393	0	FCI model; QSS heat transfer
R3	3400	900	0.208	0.393	0	FCI model; sodium vapor blanketing (Option 6); QSS heat transfer
R4	3400	900	0.208	0.393	0.1	FCI model; QSS heat transfer

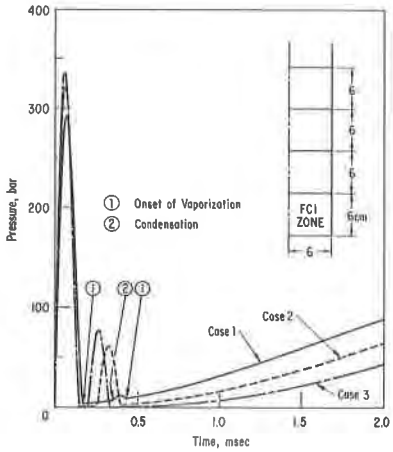

Fig. 1. Pressure history in FCI zone for cases 1, 2, and 3.

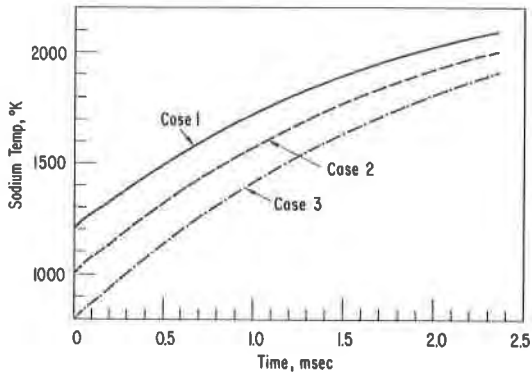

Fig. 2. Sodium temperature history in FCI zone for cases 1, 2, and 3.

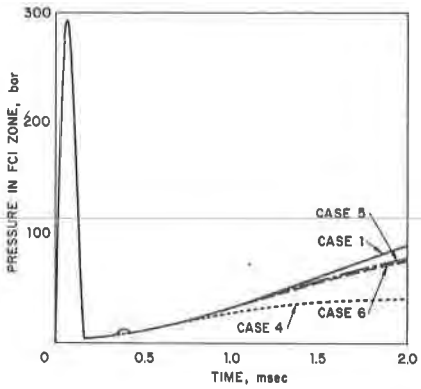

Fig. 3. Pressure history in FCI zone for cases 1, 4, 5, and 6.

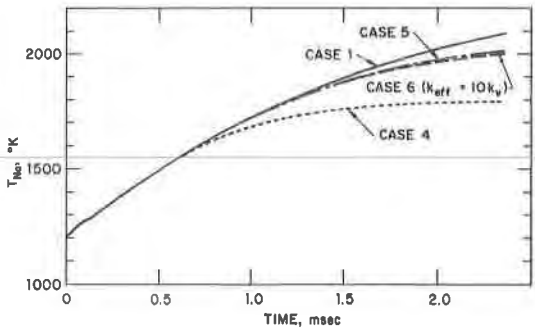

Fig. 4. Sodium temperature history in FCI zone for cases 1, 4, 5, and 6.

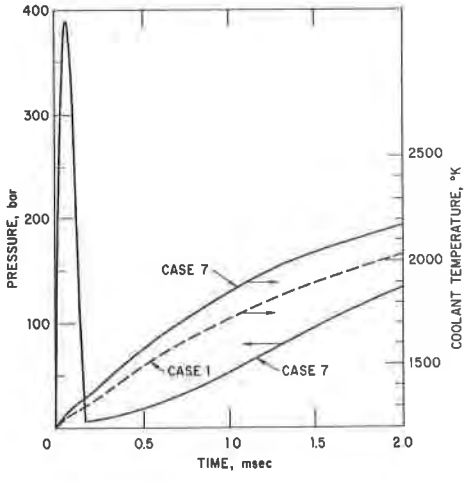

Fig. 5. Pressure and temperature history in FCI zone for case 7.

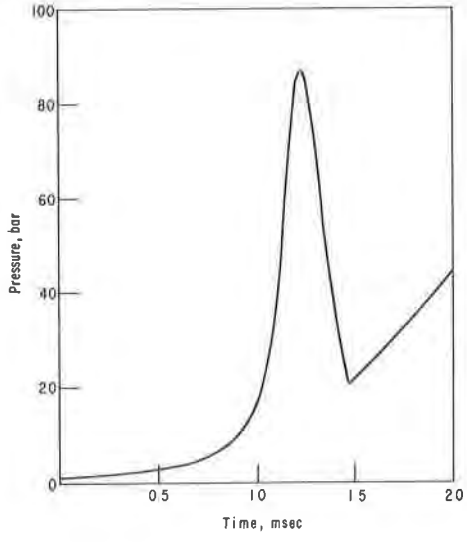

Fig. 6. Pressure history in FCI zone for case 8 (10% cushion gas).

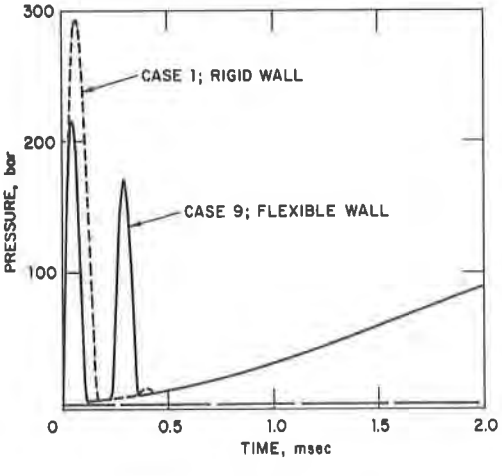

Fig. 7. Pressure history in FCI zone for cases 1 and 9.

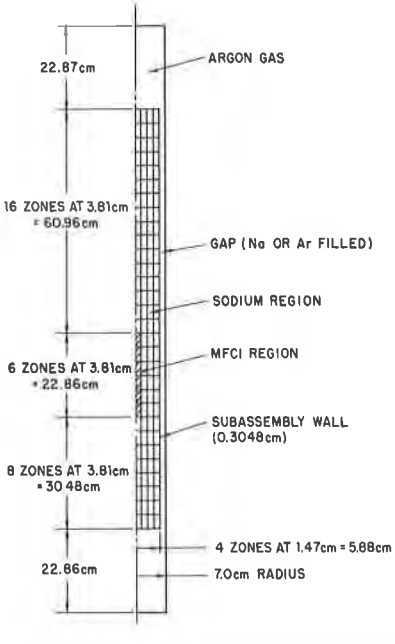

Fig. 8. Subassembly configuration.

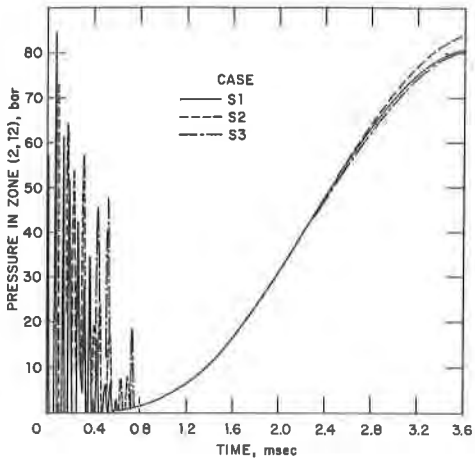

Fig. 9. Pressure history of zone (2, 12) for cases S1, S2, and S3.

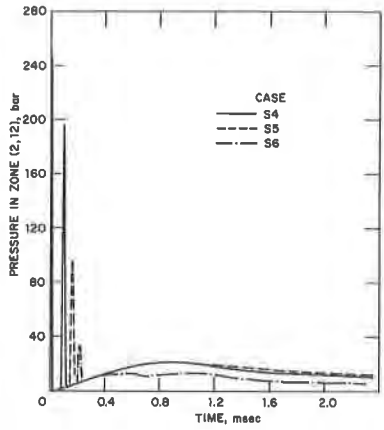

Fig.10. Pressure history in zone (2, 12) for cases S4, S5, and S6.

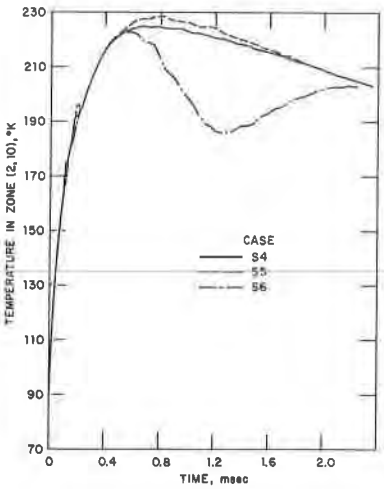

Fig.11. Sodium temperature in zone (2, 10) for cases S4, S5, and S6.

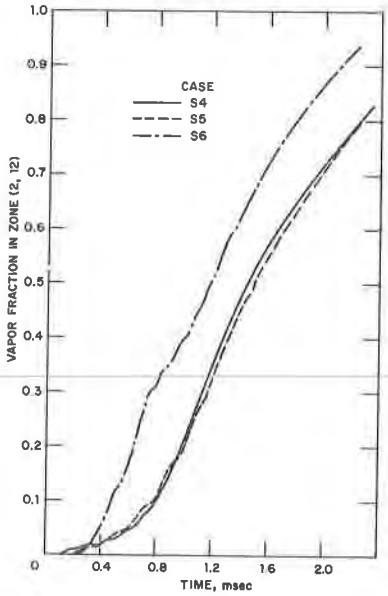

Fig.12. Sodium vapor fraction in zone (2, 12) for cases S4, S5, and S6.

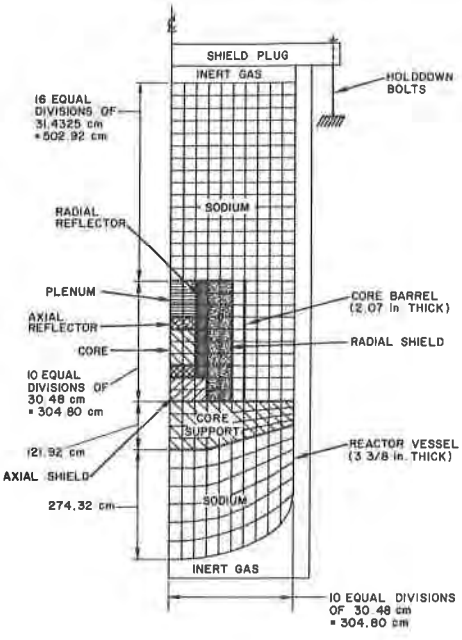

Fig.13. Full reactor configuration.

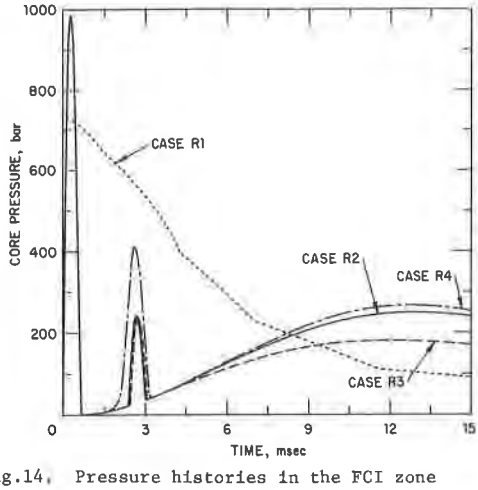

Fig.14. Pressure histories in the FCI zone (zone 2, 15) for the full reactor configuration.

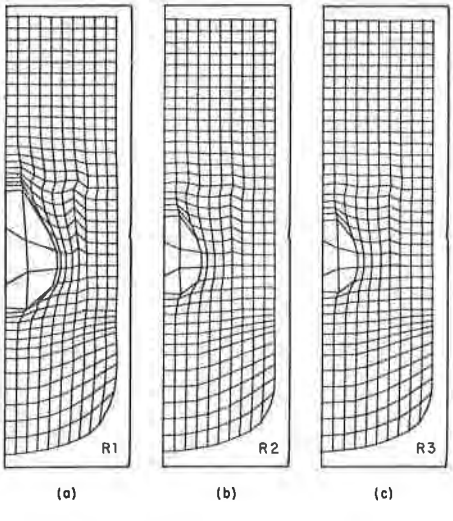

Fig.15. Deformation of Langrangian grid at time t=17.5 ms for cases R1, R2, and R3.

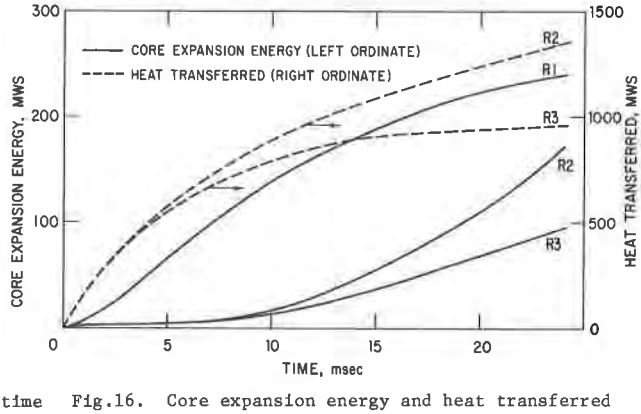

Fig.16. Core expansion energy and heat transferred for cases R1, R2, and R3.